Petroleum Science 21 (2024) 4141–4152

Contents lists available at ScienceDirect

Petroleum Science

journal homepage: www.keaipublishing.com/en/journals/petroleum-science

Original Paper

Emulsion properties and plugging performances of active crude oil enhanced by amphiphilic Janus nanosheets

Hai-Rong Wu [a, b, 1, *], Geng-Lin Li [c, 1], Guo-Rui Xu [d], Jia-Wei Chang [c], Kun-Peng Hou [a, b], Wen-Hao Shao [a, b], Ji-Rui Hou [a, b, **]

[a] State Key Laboratory of Petroleum Resources and Engineering, China University of Petroleum (Beijing), Beijing, 102249, China
[b] Unconventional Petroleum Research Institute, China University of Petroleum (Beijing), Beijing, 102249, China
[c] College of Science, China University of Petroleum (Beijing), Beijing, 102249, China
[d] COSL Production Optimization, China Oilfield Services Limited, Tianjin, 300452, China

ARTICLE INFO

Article history:
Received 1 March 2024
Received in revised form
25 July 2024
Accepted 26 July 2024
Available online 27 July 2024

Edited by Yan-Hua Sun

Keywords:
Active crude oil
Amphiphilic janus nanosheets
Emulsion
Synergistic effect
Water plugging

ABSTRACT

Inadequate strength and stability of active crude oil emulsions stabilized by conventional surfactants always lead to a limited plugging rate of plugging agents. Thus, to address this issue, the synthesis of amphiphilic Janus nanosheets was effectively carried out for enhancing the system performances and subsequently characterized. Based on the outcomes of orthogonal tests, an assessment was conducted on the nanosheet and surfactant formulations to optimize the enhancement of emulsion properties. The experimental demonstration of the complex system has revealed its remarkable emulsifying capability, ability to decrease interfacial tension and improve rheological behavior at high temperature (80 °C) and high salinity (35,000 ppm) conditions. Involving probable mechanism of the system performance enhancement is elucidated by considering the synergistic effect between surfactants and nanosheets. Furthermore, variables including water-to-oil ratio, salinity, temperature and stirring intensity during operation, which affect the properties of prepared emulsions, were investigated in detail. The efficacy and stability of the complex system in obstructing medium and high permeability cores were demonstrated. Notably, the core with a high permeability of 913.58 mD exhibited a plugging rate of 98.55%. This study establishes the foundations of medium and high permeability reservoirs plugging with novel active crude oil plugging agents in severe environments.

1. Introduction

As the development of the petroleum industry, worldwide fields have moved forward into the middle and later stages of high water cut production, and there exists an increasing trend in the presence of high-permeability water channels (Bai et al., 2000; Alfarge et al., 2017; Zhou et al., 2017). The majority of the water injected through the injection wells has become quickly extracted from the oil wells via these large pores without effectively replacing the crude oil, which hints at a crucial concern of inefficient or ineffective water circulation (Di Lullo et al., 2002; Seright et al., 2003). Simultaneously, the implementation of long-term conventional water flooding exacerbates the heterogeneity of reservoirs and causes variations in fluid mobility. The phenomenon may outcome the emergence of preferential pathways that offer minimal resistance to the injected fluid, facilitating the removal of hydrocarbons. Consequently, it might give rise to readily water breakthroughs, bringing about the formation of water channeling, water cones and fingering (Wijeratne and Halvorsen, 2015; Crespo et al., 2014). These occurrences contribute to the wastage of water resources, significantly augment the effort required for dewatering the extracted fluid, diminish the sweep efficiency, impede crude oil recovery, and ultimately reduce economic benefits (Kadeethum et al., 2017). Hence, water plugging appears to be an essential objective within the oilfield production procedure.

* Corresponding author. State Key Laboratory of Petroleum Resources and Engineering, China University of Petroleum (Beijing), Beijing, 102249, China.
** Corresponding author. State Key Laboratory of Petroleum Resources and Engineering, China University of Petroleum (Beijing), Beijing, 102249, China.
E-mail addresses: wuhairong-123@163.com (H.-R. Wu), houjirui@126.com (J.-R. Hou).
[1] These authors contributed equally to this work.

https://doi.org/10.1016/j.petsci.2024.07.026

Since the oilfield transitions into the period of high-water content or extra high-water content exploitation, the challenges associated with water flooding are becoming increasingly intricate (Seright et al., 2003; Hill et al., 2012). Developing a more adaptable and high-performing chemical water plugging agent has emerged as a crucial factor in enhancing the potential for extracting residual oil from reservoirs. Sealants or plugging agents are strategically positioned in areas of minimal resistance, leveraging the inherent properties of materials to effectively fill high-permeability channels and fractures, thus achieving flow diversion and increased sweep efficiency (Crespo et al., 2014; Kabir, 2001; Yang, 2014). Currently, a range of chemical plugging agents, including resins (Cui et al., 2022; Lai et al., 2022), gels (Tong et al., 2022; Zhang et al., 2018), particles (Li et al., 2022; Song et al., 2021; Wang et al., 2021), emulsions (Chen et al., 2014; Yu et al., 2018b), and foams (Chen et al., 2021; Seddiqi et al., 2023), etc., have been extensively documented as conceivable strategies for addressing the issues of early water breakthrough and fingering. Among these approaches for plugging in medium to high permeability reservoirs, the utilization of active crude oil in conformance control treatments demonstrates considerable potential as an effective method and exhibits unique advantages (Cui, 2015). The active crude oil experiences dissolution upon entering the oil-bearing layers and is subsequently discharged during regular production. However, when introduced into the high water-bearing layers, it undergoes spontaneous emulsification, triggering the emulsion formation, which effectively obstructs the high-permeability channel. It should be noted that the remarkable oil-water selectivity effectively safeguards the oil production capacity and controls the functioning of oil wells containing high water-bearing layers. Furthermore, the plugging agent possesses the attributes of cost-effectiveness in construction and environmental sustainability (Zhang et al., 2020).

In practice, the nature of the blockage process for active crude oil serves as emulsion water plugging. Hence, the application of active crude oil exhibits numerous benefits akin to those reported from emulsion water plugging (Bai et al., 2000; Romero et al., 1996; Vidrine et al., 2000). The water plugging of emulsion is mainly achieved through the following mechanisms (Yu et al., 2018a): (a) droplets accumulate in narrow parts of the pore channel and form a physical blockage; (b) the adsorption of active oil prompts the change of rock wettability from hydrophilic to lipophilic, which further aggravates the flow resistance of water; (c) by virtue of the "Jamin" effect and capillary resistance, emulsions demonstrate the ability to enhance mobility control and minimize core permeability, thereby facilitating the plugging of layers that feature high permeability (Soo and Radke, 1984a, 1984b). The enhanced flooding capabilities into the deeper formation exhibited by the systems allow for impeding fluid flow effectively while minimizing the need for large differential pressure (McAuliffe, 1973a, 1973b). Furthermore, emulsions are generally related to reduced formation damage, primarily given that they are not inherently a permanent plugging method and can be reversed by employing some means to achieve de-emulsification. In addition to the aforementioned benefits commonly associated with O/W emulsions which have been widely investigated (Chen et al., 2014; Moradi et al., 2014), it is noteworthy that the active crude oil possesses a tendency to spontaneously emulsify inside the formation, resulting in the formation of W/O emulsions characterized by increased viscosity and improved plugging efficacy.

Nevertheless, it is imperative to recognize the limitations of emulsions while employing active crude oil plugging agents. The conventional active substances in the emulsion systems are typically subject to certain inherent restrictions, involving degradation and agglomeration under high-temperature and high-salinity environments, corrosion of pipelines, adsorption, retention, or even fouling in reservoirs. Consequently, the resulting emulsions might fail to satisfy enduring and consistent plugging requirements in intricate reservoir environments (Kumar and Mandal, 2017; Shams et al., 2024; Ghannam, 2005). Given the increasingly complex tertiary oil recovery process, the emulsion plugging agent must exhibit both high plugging efficiency and maintain its stability under harsh conditions, such as high temperature and high salt. This places greater demands on the selection of emulsifiers and the construction of stable emulsion systems under formation conditions.

In recent years, there has been a notable surge of interest within the scientific community regarding Janus nanomaterials (Song and Chen, 2014; Xiang et al., 2020; Hu et al., 2012; Pang et al., 2014). These materials, named after the Roman deity Janus who possessed two faces, have garnered attention primarily due to their anisotropic properties. Of particular significance is the exceptional stability exhibited by Pickering emulsions when stabilized by Janus nanomaterials (Aveyard, 2012; Jia et al., 2021; Xie et al., 2020). It has been extensively investigated that amphiphilic Janus nanomaterials exhibit a greater Gibbs free energy of adsorption in comparison to conventional surfactants and particles, conferring enhanced activity and mechanical strength to the interface, giving rise to the formation of kinetically and thermodynamically stable systems (Aveyard, 2012; Bizmark et al., 2020; Glaser et al., 2006; Zahn and Kickelbick, 2014). Given that, the outstanding durability has sparked a fascination with exploring the behavior of emulsions under severe environmental conditions. However, there is a scarcity of research pertaining to the assessment of properties and plugging efficacy of active crude oil emulsions subsequent to the introduction of amphiphilic Janus nanomaterials.

Herein, amphiphilic Janus nanosheets with varying lengths of carbon chains on the hydrophobic side were prepared and characterized. Different lipophilic surfactants were chosen to form complexes with the nanosheets. The optimal combination of nanosheets and surfactants at specific concentrations, was determined based on the outcomes of the designed orthogonal tests, with a preference for the combination that yielded the highest performance in the Pickering emulsions. This paper explores the synergistic effects of nanosheets and surfactants on the enhancement of active crude oil emulsions focusing on the ability of these components to reduce interfacial tension and induce modifications to rheological properties, etc. Furthermore, an investigation was conducted on the regulations pertaining to the impact of certain variables in the emulsion fabrication procedure on the stability of the emulsions. Finally, the simulations to evaluate the efficiency and duration of the active crude oil emulsion system in effectively plugging medium and high permeability formations were conducted in the laboratory.

2. Experimental details

2.1. Materials

Styrene (St), maleic anhydride (MA), azodiisobutyronitrile (AIBN), (3-aminopropyl) triethoxysilane (APTES), tetraethyl orthosilicate (TEOS), sorbitan monostearate (Span 60), sorbitan monooleate (Span 80), and 1-(hydroxyethyl)-2-(8-heptadecenyl) imidazoline oleate (IMO) were purchased from Aladdin Reagent Co., Ltd. (Shanghai, China). Decyltriethoxysilane, dodecyltriethoxysilane, hexadecyltriethoxysilane, octadecyltriethoxysilan, and sodium alkylbenzene sulfonate (OBS-50) were purchased from Ruida Henghui Technology Development Co., Ltd. (Beijing, China). Toluene, *n*-decane, dimethylsiloxane, and ethanol were purchased from Sinopharm Chemical Reagent Co., Ltd. (Shanghai, China). Hydrochloric acid (HCl, 30%) and sodium hydroxide were

purchased from Huawei Ruike Chemical Co., Ltd. (Beijing, China). Deionized water was obtained through a Direct-Q-8UV-R Merck Millipore ultra-pure water integrated system (Millipore Corp., USA, resistance 18.2 MΩ·cm at 25 °C). The formation water used in this study is a simulated solution with a salinity of 35,000 ppm and its composition is presented in Table 1. The composition of the crude oil utilized is displayed in Table 2, and the viscosity of crude oil utilized is measured to be 3.43 mPa·s at 80 °C.

2.2. Fabrication and characterization of amphiphilic Janus nanosheets

The amphiphilic Janus nanosheets were synthesized by applying the self-assembled sol-gel method at the emulsion interface. An O/W emulsion was first constructed as a reaction vessel for the synthesis, followed by a sol-gel reaction at the emulsion interface to generate hollow silica spheres. By shattering the hollow spheres, Janus nanosheets were finally obtained. The synthesis process was adjusted based on the previous research (Chen et al., 2012; Jin et al., 2008), and the synthesis details can be found in the Supporting Information. To confirm the successful preparation of nanosheets, the surface morphology of the materials was examined using scanning electron microscopy (SEM) and transmission electron microscopy (TEM). The presence of functional groups, as well as the overall wettability properties and elemental composition of the nanosheets were verified using Fourier transform infrared (FT-IR) spectrum, energy dispersive X-ray (EDX), and contact angle (CA) measurements. Furthermore, the thermal stability of the nanosheets was evaluated using thermogravimetric analysis (TGA). Details regarding the characterization instruments and operational procedures can be located in the Supporting Information.

2.3. Preparation of emulsions stabilized by nanosheets and surfactants

The primary determinants influencing the development of the plugging system involve nanosheets, surfactants, nanosheet concentration, and the ratio of nanosheets to surfactants. Hence, the $L_{16}(4^5)$ orthogonal table could be employed to design orthogonal experiments, enabling the identification of the optimal emulsion formulation through choosing four levels for each factor. Specific factors and levels involved in the tests are shown in Table S1 in the Supporting Information. A complete set of 16 emulsion groups was developed based on the factor-level combinations specified in the orthogonal experimental table (exhibited in Table S2 in the Supporting Information). Emulsions were prepared using 35,000 ppm brine, with an oil-to-water ratio of 3:7 and a stirring rate of 500 rpm achieved by a digital ultra Turrax (T18, IKA, Germany). Additionally, the operation was carried out at room temperature. It should be noted that the evaluation criteria for the emulsions included the degree of emulsification and their temperature resistance. Precisely, the viscosity of the prepared emulsions was measured utilizing a Brookfield viscometer (DV2T, Brookfield, USA), while the droplet size was observed by an optical microscope (BX53, Olympus, Beijing). Following this, the emulsions were individually transferred into measuring cylinders with stoppers and subjected to 80 °C in an oven (KH55AS, Shanghai) to assess their temperature resistance. Finally, the optimal components of the active crude oil plugging system were determined by considering the results obtained from orthogonal experiments.

Table 1
Composition of simulated formation water.

Ionic type	$Na^+ + K^+$	Mg^{2+}	Ca^{2+}	SO_4^{2-}	Cl^-	HCO_3^-	Total
Concentration, mg/L	10686	1211	439	1619	19457	226	35000

Table 2
Composition of the crude oil.

Acidity, mg KOH/g oil	Composition, %			
	Asphaltenes	Resins	Aromatics	Saturates
0.07	0.01	4.25	15.43	80.31

2.4. Synergistic effect of nanosheets and surfactants in emulsion formation

Three sets of controlled experiments were devised to verify the synergistic effect of nanosheets and surfactants in emulsion formation. The aqueous phase consisted of brine with a concentration of 35,000 ppm, while nanosheets, surfactants, and complex systems were added to the oil phase, respectively. The viscosity–temperature curves for the three groups of emulsions were determined through experimental measurements. Under identical temperature conditions, the size and distribution of the emulsion droplets were observed. The emulsions were subsequently subjected to 80 °C to monitor the temporal evolution of oil precipitation and assess their resistance to temperature-induced destabilization over an extended period.

Additionally, an interfacial tensiometer (TX-500C, Beijing) was employed to measure the interfacial tension (IFT) for brine/crude oil, brine/active crude oil with surfactants, brine/active crude oil with nanosheets, as well as brine/active crude oil with complexed systems. Based on the rotary droplet method, the tension at the water/oil interface was determined at 80 °C and a speed of 6000 r/min. The formula for calculating IFT is shown as follows (Perles et al., 2018):

$$\gamma = \frac{\Delta\rho\omega^2 r^3}{4} \quad (L/D \geq 4) \tag{1}$$

where γ is the interfacial tension, N/m; ω is the angular velocity, rad/s; r is the short-axis radius of the oil droplet, m; $\Delta\rho$ is the difference between the densities of oil and water, kg/m^3; L is the axial diameter of the centrifuge tube, m; and D is the radial diameter of the centrifuge tube, m.

What seems beyond dispute is that the rheological properties of the emulsion indicate its capacity to function as a barrier during subsurface transportation. Thus, the storage and loss modulus (G' and G'') of the emulsions were examined utilizing a rheometer (MCR 72/92, Anton Paar, Shanghai) with the aqueous phase as simulated formation brine, and the oil phase with the addition of nanosheets, surfactants, and complexed systems, respectively. Moreover, it should be noted that all emulsions involved in this section were formulated with an oil-to-water ratio of 3:7, a temperature of 20 °C, and a stirring intensity of 500 rpm.

2.5. Exploration of variables affecting the properties of prepared emulsions

The impacts of oil-to-water ratio, aqueous mineralization, temperature, and stirring intensity during preparation on the properties of the emulsions formed were investigated. In the study of the influence of oil-to-water ratio on emulsion performances, the water content in emulsion was varied at values of 50%, 60%, 70%, 80%, and 90%. Alongside the utilization of deionized water, simulated formation brine with varying mineral concentrations of 5000, 15,000, 25,000, and 35,000 ppm were prepared as the aqueous phase to conduct a comparative characteristic analysis of the

resulting Pickering emulsions. Furthermore, five experimental trials were conducted to produce emulsions, wherein the temperature was systematically raised from 20 to 80 °C, with a gradient of 15 °C. Regarding to the stirring rate, the intensity was set at 250, 500, 1000, 1500, and 2000 rpm.

Throughout each emulsion preparation procedure, the blade of the machine is maintained at a uniform distance from the bottom of the beaker containing the oil to ensure consistency. The aqueous phase was then gradually introduced into the container until 90 s, while ensuring continuous stirring for 3 min. A portion of the emulsion was transferred into a measuring cylinder, and the instantaneous stage of its preparation was photographed using a digital camera. The viscosity was then measured, the emulsion droplets sizes as well as the distribution of the emulsion droplets were determined employing the Olympus optical microscope. Additionally, the variations in the amount of oil precipitation (oil precipitation rate) over time at 80 °C were subsequently documented. When figuring out how each factor affected how the emulsion performed, the conditions of the other parameters were kept as fixed as possible. Besides, all of the oil phases that manufactured emulsions throughout the experiments conducted in this section were maintained at a constant level of specific concentrations of nanosheets and surfactants that were previously determined.

2.6. Evaluation of plugging performances for active crude oil

Core displacement experiments were implemented to evaluate the plugging effectiveness of active crude oil complexed with nanosheets and surfactants at 80 °C and salinity of 35,000 ppm. The schematic diagram of multifunctional core displacement device utilized is depicted in Fig. S1 in the Supporting Information. Initially, the cores were saturated with brine and crude oil. The cores endured aging at 80 °C for 24 h with the intent to achieve a uniform distribution of oil and water within the cores. Following the initial stage of primary water flooding, the pump was halted. Subsequently, a reverse injection of 0.5 pore volume (PV) of active crude oil was conducted. After a period of 3 h for aging, secondary water flooding was started. This process continued until the water cut at the outlet exceeded 98%, and the pressure reached a stable state. Afterwards, the water flooding was extended for a duration of 5 h to assess the flushing resistance of the plugging agent. The breakthrough pressure and the variations in pressure over time subsequent to the beginning of secondary water flooding, were recorded. All the experiments were operated at 80 °C, and the injection rate was 0.1 mL/min. Furthermore, the plugging rate and residual resistance factor (RRF) were calculated based on the obtained data. Parameters of the cores used are exhibited in Table 3. Darcy-Weisbach formula depicted in Eq. (2) is used to determine the permeability of the core (Yue et al., 2022). Besides, formulas for the plugging rate and the residual resistance factor are shown as Eqs. (3) and (4), separately (Yuan et al., 2023):

$$K_n = \frac{100Q\mu L}{A(P_1 - P_2)} \tag{2}$$

$$E_w = \frac{K_0 - K_1}{K_0} \tag{3}$$

$$F_{RR} = \frac{K_0}{K_1} \tag{4}$$

where K_n is the permeability, mD; μ represents the viscosity of the fluid, mPa·s; L is the length of the core, cm; A is the cross-sectional area of the core, cm^2; P_1 and P_2 are the pressures at the inlet and outlet of the core, respectively, MPa; E_w is the plugging rate, %; F_{RR} is the residual resistance factor; K_0 is the permeability before plugging, mD; K_1 is the permeability after plugging, mD.

3. Results and discussion

3.1. Synthesis and characterization of amphiphilic Janus nanosheets

In the study, the sol-gel method was employed at the emulsion interface for the synthesis of amphiphilic Janus nanosheets (Chen et al., 2012, 2020; Xu et al., 2017). The silane coupling agents underwent interactions, resulting in the grafting of amines and straight-chain alkanes on both sides of the nanostructures. The sol-gel process is both ecologically sustainable and time-efficient, and the yield of nanosheets can exceed 20%. Four produced nanosheets are referred to as Janus-L10, Janus-L12, Janus-L16, and Janus-L18, respectively, based on the varying lengths of the hydrophobic chain segments to which the nanosheets are attached. Fig. 1 illustrates the schematic of the synthesis process.

SEM and TEM images (see Figs. S2 and S3 in the Supporting Information) provide unambiguous evidence of the flake-like structure of the product, with nanosheets with thicknesses ranging from 30 to 80 nm. The infrared spectra in the wavenumber range of 500–4000 cm^{-1} regarding the Janus nanosheets prepared are shown in Fig. S4 in the Supporting Information. The evidence that the appearance of characteristic peaks corresponding to amino and alkyl groups were obviously detected manifests that hydrophilic and hydrophobic chain segments were successfully grafted upon the opposite sides of the nanosheets. All four nanosheets exhibited three phases of weight loss in the TGA curves (Fig. S5 in the Supporting Information), representing the weight loss of adsorbed water, amino group and alkyl group, respectively, which presents proof supporting the successful grafting of functional groups. According to the EDX results (Fig. S6 in the Supporting Information), a successful synthesis of the product is evidenced by the identification of the critical elements carbon (C), nitrogen (N), oxygen (O), and silicon (Si). Furthermore, after pressing the powders of the synthesized nanosheets into circular flakes, their three-phase contact angles were measured using the sessile drop method and shown in Fig. S7 in the Supporting Information. Each of the four nanosheets demonstrated contact angles exceeding 90°, with values ranging from 115° to 125°. The nanosheets exhibited a lipophilic nature, consistent with the expectation of the nanosheet synthesis process for modifying the HLB value. These outcomes also provide compelling evidence for the effective attachment of hydrophobic carbon chains.

Table 3
Physical parameters of the cores used.

Core No.	Length, cm	Permeability, 10^{-3} μm^2	Porosity, %	Original oil saturation, %
1	30.05	308.64	20.51	67.9
2	30.18	599.65	22.24	71.2
3	29.95	913.58	25.15	73.1

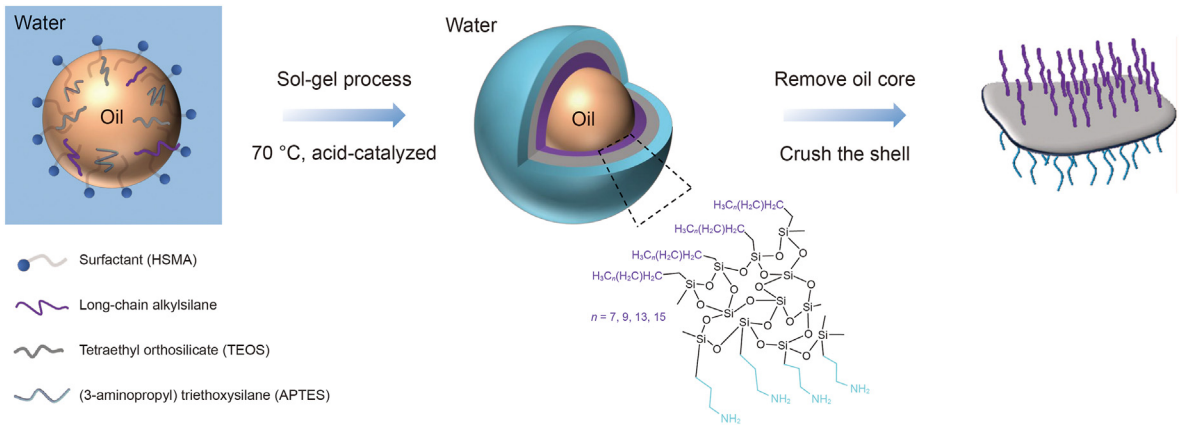

Fig. 1. Scheme of the fabrication for Janus nanosheets.

3.2. Implementation of orthogonal tests to determine optimal active oil system

Pickering emulsions stabilized with varying concentrations of nanosheets and surfactants were prepared using the factor level combinations outlined in the $L_{16}(4^5)$ orthogonal experimental table. The viscosity data for each set of emulsions were recorded and presented in Table S3 in the Supporting Information. Meanwhile, the emulsion droplet images can be seen in Fig. 2(a). The evidence that the emulsion droplets demonstrate a diminutive size as well as a consistent distribution manifests that the emulsifier employed exhibits a high degree of emulsifying capability, resulting in a well-formed emulsion. All sixteen emulsions prepared were water-in-oil emulsions. It was evident that the phenomenon of emulsion microphotographic reflection and the measurement of emulsion viscosity basically correspond to each other. The emulsions of OBS-50 family all produced poor emulsification effect. Notably, group 4 exhibited the smallest droplet size, measuring within 5 μm. Additionally, this emulsion demonstrated the highest viscosity and the most favorable degree of emulsification. The emulsions were subjected to a thermal treatment at 80 °C for 3 days (as shown in Fig. 2(b)). By examining the water precipitation state of the emulsions, distinct trends of varying temperature resistance were observed within these groups. Among the tests, it was discovered that both Span 60 and Span 80 stabilized emulsions exhibited partial demulsification. Furthermore, the temperature resistance of Span 80 stabilized emulsions was marginally superior to that of the Span 60 series. However, the OBS-50 stabilized emulsions demonstrated poorer temperature resistance, ultimately resulting in complete demulsification for all four groups. The emulsions stabilized by IMO showed minimal demulsification and proved favorable durability under elevated temperatures, thereby satisfying the demands of high-temperature and high-salinity reservoir applications.

The viscosity data were utilized as an indicator to assess the efficacy of emulsification. Meanwhile, a range analysis method was developed to evaluate the orderly significance of factors influencing the index and to identify the optimum combination of the levels (Liu J. et al., 2023; Liu et al., 2022). Table 4 displays the results of the range analysis. It should be noted that the primary criteria for evaluation encompass the calculated k_j and R_j values. The analysis method commences by calculating the average value of each index associated with a specific level of the factor. Then, the aforementioned procedure for other levels of this factor is performed to acquire k_j values (K_j values shown in Table 4 are data that are not averaged out). The calculation of the R_j values, referred to as the range value of each design factor, involves the difference between the maximum and minimum k_j values.

Single index assessment in the orthogonal tests reveals that the range magnitude of the four factors follows the order $R_B > R_C > R_D > R_A$. This implies that the variables influencing the viscosity index of the emulsions are ranked as follows: surfactant type, nanosheet concentration, concentration ratio of nanosheets to surfactants, and nanosheet type. In accordance with the method of analyzing the data, the selection of a surfactant significantly impacts the characteristics of the resulting emulsion. The optimal choice, as determined by range analysis, was found to be A_4, B_4, C_4, and D_4, which involves the use of 0.3 wt% Janus-L18 and 1.2 wt% IMO. Among the 16 groups, the emulsion performance was proven to be most favorable in group 4, specifically with the addition of A_1, B_4, C_4, and D_4, *i.e.*, a combination consisting 0.3 wt% Janus-L10 and 1.2 wt% IMO. The emulsions produced by this group presented a viscosity of 4480 mPa·s. Thus, a comparative experiment was conducted to assess the emulsion performance of the preferred system by comparing its results with those obtained from the fourth group subsequently.

The W/O emulsion was prepared in accordance with the formulation that was determined based on the results obtained from the analysis of orthogonal experimental data. The measured viscosity of the emulsion was determined to be 6000 mPa·s, surpassing the values from the experimental trials conducted by group 4. In Addition, the emulsion droplets that were generated showed a tiny size and a uniform distribution. Simultaneously, the emulsion exhibited positive temperature resistance and maintained its stability over 3 days. The photographs involving are shown in Fig. S8 in the Supporting Information. Consequently, the development of the active crude oil plugging system reached its conclusion, with the selection of 0.3 wt% Janus-L18 and 1.2 wt% IMO.

3.3. Synergistic effect of nanosheets and surfactants in enhancing emulsion properties

The role of amphiphilic Janus nanosheets in enhancing the performance of emulsions in high-temperature and high-salt formations is worth exploring. Hence, the experimental analysis focused on the impact of amphiphilic Janus nanosheets on improving emulsion stability, interfacial activity, and rheological properties when combined with surfactants. Finally, the mechanism of those two components in improving the emulsion properties was illustrated.

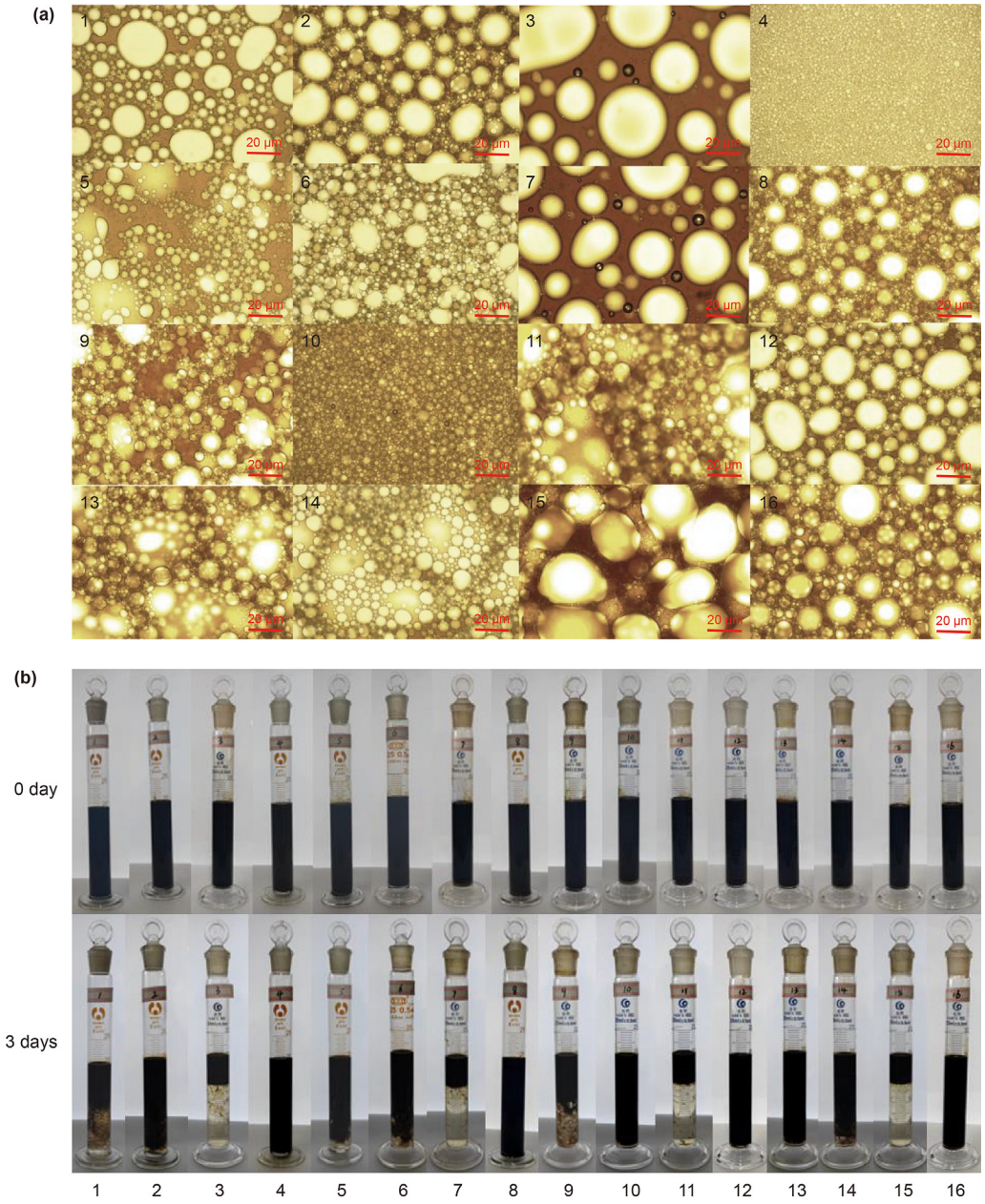

Fig. 2. Microscopic images of emulsion droplets for 16 groups of Pickering emulsions prepared (**a**), and photographs captured before and after subjecting the emulsions to a thermal treatment in an oven at 80 °C for 3 days (**b**).

Table 4
Analysis of emulsion viscosity index data.

	Nanosheet type (A)	Surfactant type (B)	Nanosheet concentration (C)	Concentration ratio (nanosheets: surfactants) (D)
K_1	11365	12550	10095	10555
K_2	10455	12650	10795	11175
K_3	10875	6675	11320	10480
K_4	12615	13435	13100	13100
k_1	2841.25	3137.5	2523.75	2638.75
k_2	2613.75	3162.5	2698.75	2793.75
k_3	2718.75	1668.75	2830	2620
k_4	3153.75	3358.75	3275	3275
R_j	540	1690	751.25	655

3.3.1. *Emulsification efficiency and emulsion stability*

Fig. 3 illustrates the viscosity–temperature profiles of emulsions stabilized by 0.3 wt% Janus-L18, 1.2 wt% IMO, and the complex, respectively. Actually, the viscosity–temperature relationship of an

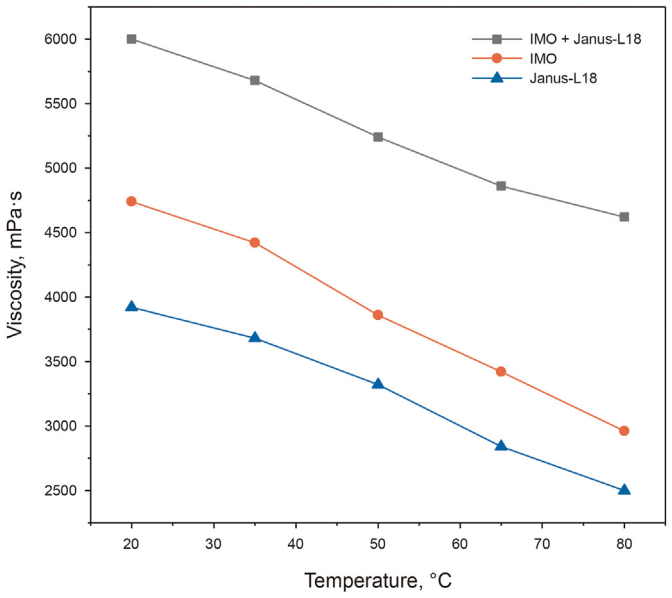

Fig. 3. Viscosity versus temperature for emulsions stabilized by IMO, Janus-L18, and the complex.

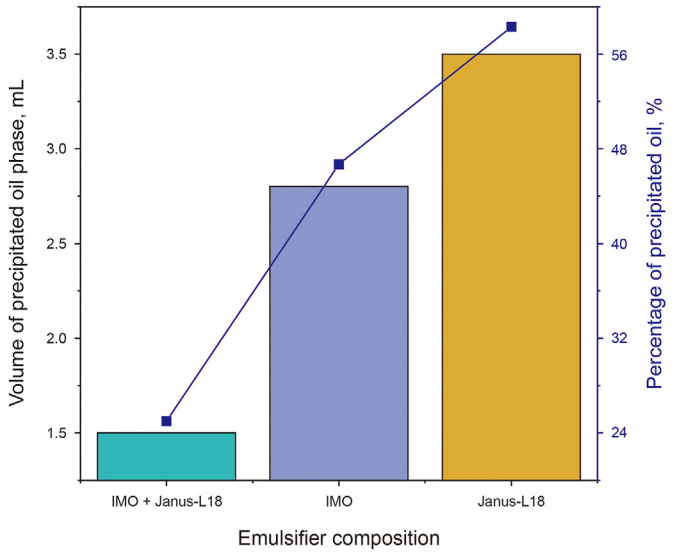

Fig. 4. Oil precipitation after storage of 72 h at 80 °C for emulsions stabilized by IMO, Janus-L18, and the complex.

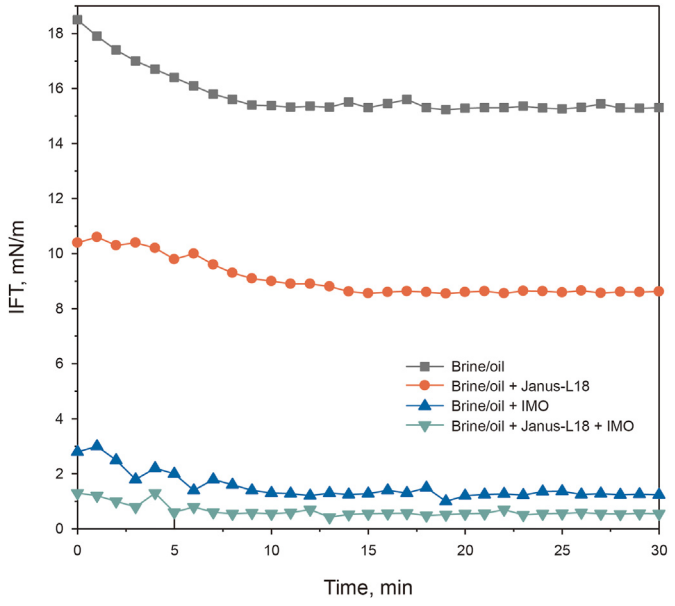

Fig. 5. Interfacial tension of brine/crude oil, and brine/crude oil with various active components.

emulsion serves as a macroscopic depiction of the rheological characteristics exhibited by the emulsion. Eyring (1935, 2004) declared that the definition of activation energy in fluid dynamics can be conceptualized as the minimal amount of energy necessary to induce the formation of a cavity within the fluid, thereby enabling the exchange of positions between a molecule and its adjacent molecule. At elevated temperatures, fluid molecules possess sufficient energy to trigger the development of cavities within the liquid, allowing their reciprocal movement. Consequently, three categories of emulsions demonstrate a similar inclination towards decreasing viscosity as the temperature rises. Simultaneously, the reduction in viscosity of a W/O emulsion as temperature increases might be attributed to the decline in viscosity of the oil phase when the temperature is lifted. It can be found from Fig. 3 that the viscosity of the stabilized emulsion is lower when either surfactants or nanosheets are used individually compared to when both are added concurrently at any given temperature. Furthermore, the droplet size and distribution confirm the emulsification effect reflected from this point.

Photographs of the emulsions prior to and following three-day storage at 80 °C are displayed in Fig. S9 in the Supporting Information, and the oil precipitation volume was employed as an indicator to visually assess and compare the stability of the emulsions (see Fig. 4). The oil precipitation volume refers to the quantified amount of oil that is discharged from the emulsion within a span of 72 h. Analysis results indicate that the addition of both IMO and Janus-L18 simultaneously gave rise to a lower amount of oil precipitation compared to when either component was employed individually. This suggests that the combination of the surfactants with the nanosheets improves the long-term stability of the emulsions in terms of their resistance to temperature changes.

3.3.2. *Interfacial tension reduction ability*

Interfacial tension plays a significant role in determining the stability of emulsions. This is because the development of emulsions results in an expansion of the interfacial area and an elevation of interfacial energy, both of which contribute to the heightened instability of the system (Liu R. et al., 2023). With the goal of improving the stability of emulsions, it is attainable to decrease the interfacial tension, thereby reducing the interfacial energy. The variation of IFT with time is shown in Fig. 5. The measured value for the IFT between crude oil and brine was approximately 15.3 mN/m. Upon the addition of Janus-L18 at a concentration of 0.3 wt% into the crude oil, a reduction to around 8.6 mN/m was observed. After introducing 1.2 wt% IMO as a standalone additive to the crude oil, the IFT experienced a notable decrease to 1.2 mN/m. Subsequently, when the complex system was applied with the crude oil, the IFT between the oil and water was further diminished to 0.55 mN/m. It can be noticed from the outcomes that both nanosheets and surfactants have the ability to effectively decrease the interfacial tension, whereas surfactants play a more prominent role therein. Additionally, the co-existence of nanosheets and surfactants can further enhance the reduction of IFT in a synergistic manner.

3.3.3. Rheological behavior

Plots of storage modulus and loss modulus as a function of shear frequency for emulsions stabilized by 0.3 wt% Janus-L18, 1.2 wt% IMO, and the complex are displayed in Fig. 6. The viscoelastic properties exhibited by emulsions are indicative of the rheological behavior of the interface between oil and water. These characteristics assume indispensable parts in understanding the formation, transportation, and sealing capabilities of emulsions within the pore channels and throats of formations. The values of G' and G'' in emulsions are contingent upon the "self-healing" capacity of the interface film, which refers to the potential to rapidly reconstruct itself through the migration of adjacent active substances (such as surfactant molecules or particles) when confronted with external shear forces (Barnes, 1994; Kolotova et al., 2018). From the plot, it is recognized that the emulsions involving both surfactants and nanosheets indicate higher values for G' and G'' compared to when either component is added individually. This observation aligns with the findings from the viscosity test. The storage and loss moduli of all three categories of emulsions exhibit an upward trend as the shear frequency is raised. In each group of emulsions, it is observed that the storage modulus surpasses the loss modulus, thereby suggesting that the emulsions demonstrate characteristics that are more akin to solids. Furthermore, it can be found that G' exhibits a more pronounced increase in response to shear frequency compared to G''. As the frequency of shear increases, the relaxation process of molecular diffusion between the bulk and the interface becomes shorter, which leads to a slight rise in the loss modulus, but a significant acceleration in interfacial deformation. Consequently, the intermolecular interactions at the interface are intensified, resulting in a substantial boost in the storage modulus. Therefore, the overall bulk-phase modulus of the emulsion is increased with an enhancement in oscillation frequency. Compared with the emulsion formed by surfactants or nanosheets individually, the viscoelastic properties of the emulsion were significantly improved after the synergistic effect of the two, which theoretically could significantly improve the plugging capacity of the active crude oil system.

The adhesion energy between the nano-solid material and the interface is much higher than the thermal energy, and the planar structural characteristics of the nanosheets allow for limited rotation at the interface, resulting in irreversible adsorption upon reaching the interface (Aveyard, 2012; Bizmark et al., 2020; Nonomura et al., 2004). Nanosheets demonstrate improved interfacial strength in comparison to molecular surfactants due to their inherent rigidity. When the nanosheets are arranged at the interface, a three-dimensional mesh structure is formed between the emulsion droplets, thus preventing flocculation and agglomeration with each other through steric effects (Yu et al., 2021). The hydrophilic amino groups of the amphiphilic nanosheets are oriented towards the water phase, while the hydrophobic long chains on the other side reach into the oil phase (Glaser et al., 2006). Additionally, the surfactants are positioned within the interstitial spaces between the sheets at the oil/water interface. Fig. 7 illustrates the schematic distribution of emulsifiers at the oil/water interface. Interactions between surfactants and nanosheets prolonged the duration of their stabilization on the emulsion interface without desorbing down. In their synergy, the occurrence of adsorbed nanoparticles reduces the repulsive forces between surfactant molecules, thereby resulting in an increase in the quantity of active sites (Horozov et al., 2005). Therefore, the interface is endowed with enhanced activity to minimize its tension, thus forming a thermodynamically more stable system (Kumar et al., 2013), and with lifted mechanical strength to counteract the aggregation of emulsifiers under high temperatures and sanity conditions. The presence of the inter-emulsion network architecture imparts the augmentation of the bulk-phase viscosity of the emulsions and the acquisition of solid-like characteristics, which in turn provides high performance viscosity and effective flow control even under conditions of low shear (Kawazoe and Kawaguchi, 2011).

In summary, the magnitude of the synergistic effect is not only proportional to the efficacy of emulsion generation, but also to factors such as droplet size, viscosity, viscoelasticity, and the extent of interfacial tension reduction within the emulsion. The Janus-L18 and IMO complex system has greatly enhanced the properties of the emulsions and has presented theoretical possibilities for the development of emulsion plugging in severe surroundings.

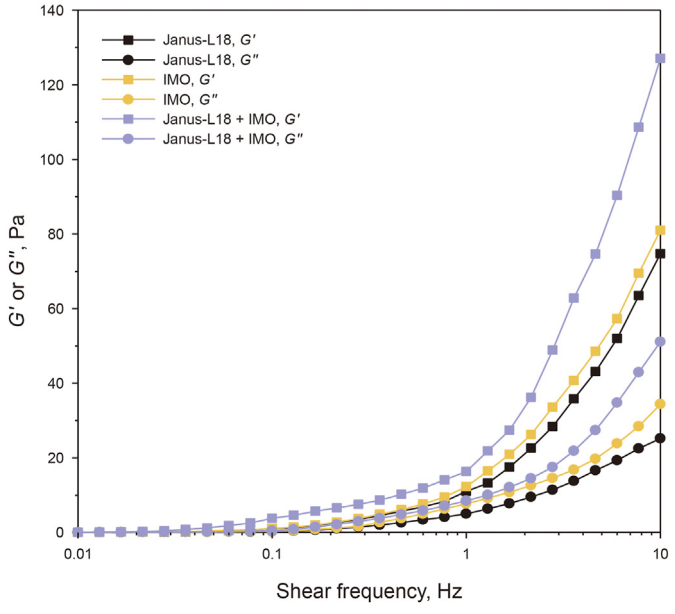

Fig. 6. G' and G'' as a function of shear frequency for emulsions stabilized by IMO, Janus-L18, and the complex system.

3.4. Regulation effect of preparation conditions on emulsion properties

3.4.1. Water-to-oil ratio

The viscosity measurements of emulsions that were prepared employing varying water-to-oil ratios can be found in Fig. 8(a). There exists a noticeable increase in the viscosity of the emulsion as the water content falls below 80%. When the water content of the emulsion reaches 90%, a decrease in viscosity occurs, accompanied by a propensity for phase transitions and demulsification. This suggests that the transition point of the emulsion should be situated within the volume fraction range of 80%–90% for the internal phase. Additionally, as the water content of the emulsion increases, there is a corresponding rise in the number of droplets comprising the emulsion, as well as a tendency for the droplet size to decrease. Meanwhile, a growth in the contact area and mutual extrusion between droplets is noted. At an oil-to-water ratio of 1:9, the emulsion exhibits a transition point characterized by a decline in both stability and emulsification effectiveness, associated with an observable increase in droplet size (Fig. S10(a) in the Supporting Information). This phenomenon is correlated with the results of the viscosity tests. After three days, the emulsion was photographed and shown in Fig. S10(b), while the percentage of precipitated oil was determined and depicted in Fig. 8(b). It can be seen that the variation law of emulsion oil precipitation rate with water content is exactly negatively correlated with the viscosity test results. Emulsions formulated with a water content of 80% indicate the best

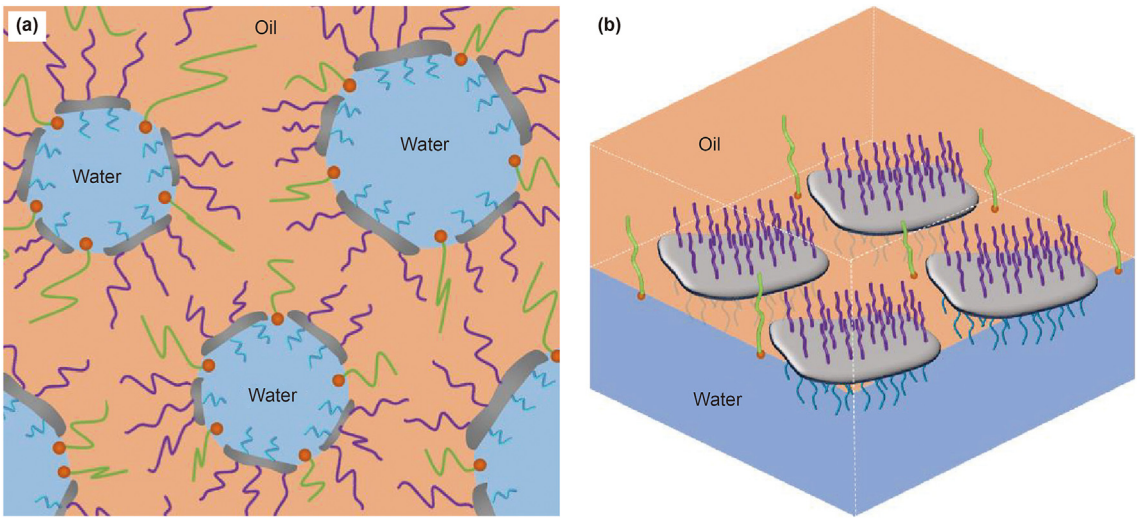

Fig. 7. Two-dimensional (**a**) and three-dimensional (**b**) schematics of distribution of nanosheets and surfactants at the oil/water interface. Green models with an orange head and a long-chain tail represent IMO surfactants. Purple and blue chains on the lamellar structure correspond to the hydrophobic and hydrophilic segments of the amphiphilic nanosheets, respectively.

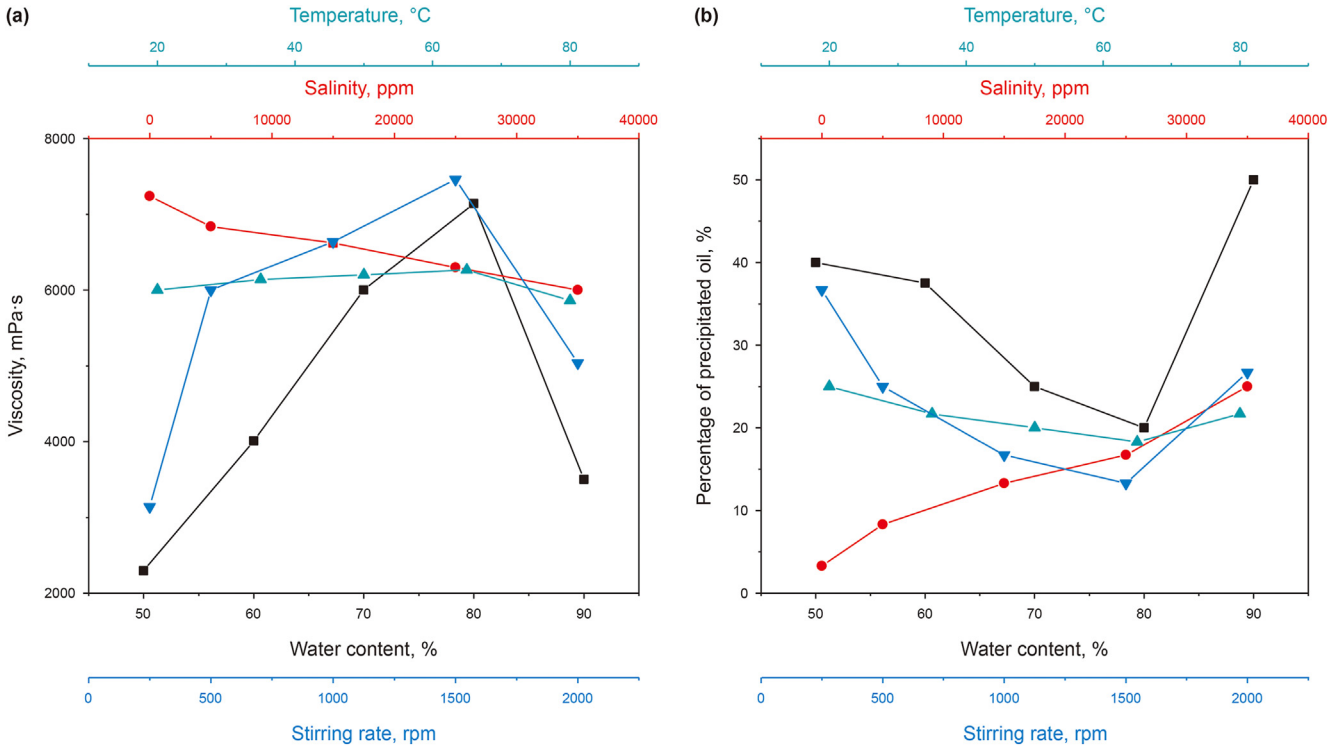

Fig. 8. Variations of viscosity (**a**) and oil precipitation percentage (**b**) in relation to water content, salinity, temperature, and stirring rate in preparation.

performance viscosity and stability characteristics.

3.4.2. Salinity of the water phase

As illustrated in Fig. 8(a), there is a reduction in the viscosity of the emulsion as the salinity grows. This phenomenon can be attributed to a minor aggregation of the active ingredients, causing a decrease in their ability to emulsify (Tang et al., 2022). However, it is worthwhile to point out that the decrease in viscosity is relatively modest within each increment of salinity. This finding suggests that while the salinity does affect the emulsification features of the system, the emulsion still demonstrates a noteworthy resistance to salt. From the data on the percentage of oil precipitation presented in Fig. 8(b), it can be seen that the stability of emulsions is observed to be superior and exhibits minor variations under different salinity conditions. Yet, the general trend still adheres to the principle that emulsion stability increases as salinity reduces. Among these groups, emulsion prepared utilizing deionized water as the aqueous phase demonstrates optimal viscosity and stability, in addition to tiny emulsion droplets that are uniformly distributed. The relevant pictures are presented in Fig. S11 in the Supporting Information.

3.4.3. Temperature in preparing emulsion

Measurements of the viscosity of the emulsions prepared under varying temperature conditions are portrayed in Fig. 8(a). Obviously, the viscosity of the emulsion exhibits an initial elevation followed by a subsequent drop as the temperature is raised, with minimal variation. Besides, it can be observed that the size of the droplet shows a reducing and subsequent increasing trend with increasing temperature, which corresponds to the results of the viscosity test (Fig. S12(a) in the Supporting Information). The emulsion prepared at 65 °C shows the highest values of viscosity and smallest droplet size. Emulsification properties are influenced by the temperature conditions during formulation, albeit to a negligible degree. It is evidenced that as the preparation temperature rises, there is a slight agglomeration of the emulsifiers, which leads to an increase in various interaction forces, such as extrusion between oil and water droplets under shear. Consequently, these interactions potentially contribute to the improved performance of the resulting emulsions (Cui et al., 2023). However, as the temperature continues to grow, the aggregation intensifies to a point where the emulsifiers can no longer be effectively stabilized at the interface, giving rise to a deterioration of the emulsification effect. The durability of the emulsions formulated under various temperature conditions reveals the remarkable temperature resistance of the emulsions constructed using the complex system. Among all the emulsions tested, the one produced at 65 °C presents the least amount of oil precipitation and best stability (Fig. 8(b)).

3.4.4. Intensity of stirring in preparing emulsion

The measurements of the viscosity for emulsions prepared under varying stirring intensities are depicted in Fig. 8(a). The viscosity exhibits a non-linear relationship with the stirring rate, beginning to rise and then falling. As can be seen, the measured trends in viscosity indicate an inverse correlation with the patterns observed in droplet size and oil precipitation as a function of stirring rate, which is consistent with the anticipated regulation (see Fig. S13(a) in the Supporting Information and Fig. 8(b)). The rate of stirring is indicative of the level of intensity in the emulsification procedure. A higher stirring rate corresponds to a greater intensity, forming more uniform emulsion droplets within the suitable range of stirring rates. This outcome is advantageous for enhancing and sustaining the dispersion of emulsified droplets, thereby leading to increased stability of the interface film. Nevertheless, if the stirring rate is insufficiently low, the intensity of mixing between the oil and internal phases is inadequate, causing poor emulsification and hindering the formation of a stable W/O emulsion system. When the stirring rate exceeds a certain threshold, more energy is introduced into the system within a given time frame. Consequently, it contributes to a reduction in the size of droplets, an increase in the overall surface area, and a higher degree of emulsification. From a thermodynamic perspective, it is observed that maintaining a constant amount of emulsifier while substantially expanding the oil/water interfacial area is susceptible to the rupture of the emulsion film, which in turn improves the instability of the system, preventing the formation of a stable emulsion system (Acevedo et al., 1985). Notably, the emulsion prepared at a stirring rate of 1500 rpm demonstrates the highest viscosity, smallest droplets and least oil precipitation among the tested conditions.

3.5. Performance of water plugging for active crude oil

The core sample was subjected to a 3-h aging process following the injection of active crude oil. Corresponding plot referred to as Fig. 9 presents the injection pressure starting from the initiation of subsequent water flooding and continuing for a duration of 5 h of continuous injection. The introduction of water into the core

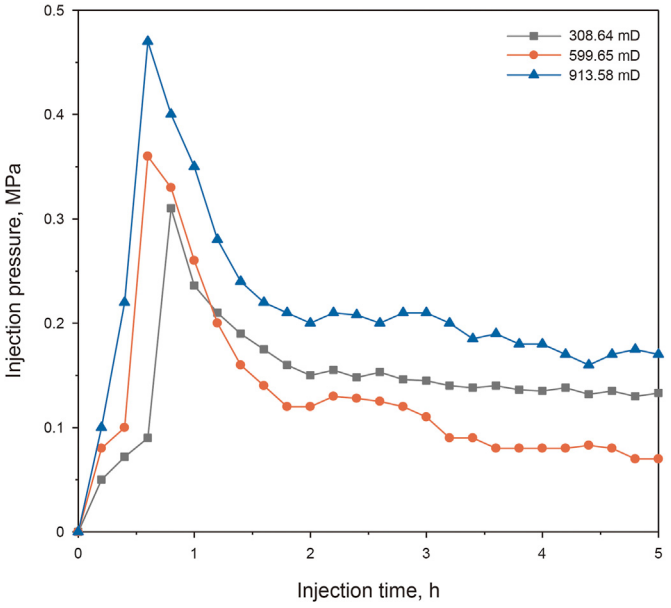

Fig. 9. Variation of injection pressure against injection time following the initiation of subsequent water flooding.

triggers the generation of a W/O emulsion with high viscosity, which obstructs the pores. Thus, it follows that a sudden rise in pressure occurs, causing a redirection of the liquid flow and expulsion of the remaining oil in the narrow channels. Subsequently, the pressure gradually decreases until it reaches a more stable state. With the continuous injection of the water phase, the pressure shows a downward trend but the rate of this process is relatively slow. The flushing resistance test confirms the duration effectiveness of the water plugging.

Experimental data pertaining to the plugging process for three distinct sets of cores of varying permeabilities are documented in Table 5. The significant decrease in permeability of the cores was evident following the injection of active crude oil, which resulted in a plugging rate exceeding 95% for all three cores. What seems beyond dispute is that the magnitude of the breakthrough pressure and RRF characterize the maximum pressure at which water breaks through in the porous medium and the extent to which the plugging agent remains in the core, respectively. These parameters reflect the effectiveness of the temporary plugging agents in reducing the permeability of the porous medium, thereby indicating the strength of the plugging agents. In the experiments, the obtained data from all three sets of cores demonstrated satisfactory results in terms of breakthrough pressure and RRF. Notably, a positive correlation was observed between the permeability of the core and the corresponding pressure and RRF values. This relationship was especially apparent for the core with a high permeability of 913.58 mD, where the breakthrough pressure and RRF were measured to be 0.47 MPa and 69.05, respectively. The phenomenon may occur due to the presence of the active crude oil and a greater amount of water present in the high permeability layer. As a result, multitude of emulsion droplets emerged through the shearing action of the formation pores, which could aggregate and obstruct the throats of the formation channels (Zhou et al., 2017; Liu R. et al., 2021, 2023).

In summary, the active crude oil plugging system composed of Janus-18 and IMO at specific concentrations demonstrates remarkable effectiveness in plugging and flushing resistance. This achievement can be attributed to the system's capability to form a stable W/O emulsion with high viscosity inside the core, forcing the

Table 5
Core plugging experimental data.

Core No.	Permeability, mD		Plugging rate, %	Breakthrough pressure, MPa	RRF
	Before plugging	After plugging			
1	308.64	15.14	95.09	0.31	20.39
2	599.65	21.40	96.43	0.36	28.02
3	913.58	13.23	98.55	0.47	69.05

diversion of the water flow. The findings of this study offer valuable theoretical insights and practical guidance for the application of active crude oil plugging agents in efficiently plugging medium and high permeability channels under high temperature and salinity environments.

4. Conclusions

On the basis of a self-assembled sol-gel method at the emulsion interface, the amphiphilic Janus nanosheets with varying carbon chain lengths were successfully synthesized. After conducting designed orthogonal experiments, the composition and concentration formulations referred to as 0.3 wt% Janus-L18 + 1.2 wt% IMO in the active crude oil plugging system were determined. In contrast to individual components, the complex system indicates a more substantial contribution to emulsification capability, stability of the developed emulsion, reduction of interfacial tension, and enhancement of rheological properties. It is worth mentioning that the oil/water IFT was significantly reduced from 15.3 to 0.55 mN/m by the synergistic effect of nanosheets and surfactants. Additionally, the properties of prepared emulsions are influenced by various factors, including the water-to-oil ratio, salinity, temperature and stirring rate employed during the preparation process. In accordance with the results, the most optimal performance of the emulsions was achieved. Of significance, the complex system demonstrated a superior plugging efficiency for cores of medium and high permeability, specifically, exhibiting satisfactory breakthrough pressure, plugging rate, and RRF. Impressively, the active crude oil system achieved a 98.55% plugging rate for the high permeability core of 913.58 mD. Therefore, this manuscript delivers a novel strategy for constructing a synergistic stabilized active crude oil emulsion by introducing amphiphilic Janus nanosheets and surfactants to meet the requirements of plugging at high-temperature and high-salinity environments.

CRediT authorship contribution statement

Hai-Rong Wu: Writing – review & editing, Supervision, Resources, Project administration, Funding acquisition, Conceptualization. **Geng-Lin Li:** Writing – review & editing, Writing – original draft, Methodology, Investigation, Formal analysis, Data curation, Conceptualization. **Guo-Rui Xu:** Writing – review & editing, Resources, Project administration. **Jia-Wei Chang:** Writing – review & editing, Methodology, Data curation. **Kun-Peng Hou:** Writing – review & editing, Methodology, Formal analysis, Data curation. **Wen-Hao Shao:** Writing – review & editing, Methodology, Formal analysis. **Ji-Rui Hou:** Writing – review & editing, Supervision, Project administration.

Declaration of competing interest

The authors declare that they have no known competing financial interests or personal relationships that could have appeared to influence the work reported in this paper.

Acknowledgements

This work was financially supported by National Natural Science Foundation of China (52374053), Beijing Natural Science Foundation (2204092), and Beijing Municipal Excellent Talent Training Funds Youth Advanced Individual Project (20180000020124G163).

Appendix A. Supplementary data

Supplementary data to this article can be found online at https://doi.org/10.1016/j.petsci.2024.07.026.

References

Acevedo, S., Méndez, B., Rojas, A., Layrisse, I., Rivas, H., 1985. Asphaltenes and resins from the Orinoco basin. Fuel 64, 1741–1747. https://doi.org/10.1016/0016-2361(85)90402-8.
Alfarge, D.K., Wei, M., Bai, B., 2017. Numerical simulation study of factors affecting relative permeability modification for water-shutoff treatments. Fuel 207, 226–239. https://doi.org/10.1016/j.fuel.2017.06.041.
Aveyard, R., 2012. Can Janus particles give thermodynamically stable Pickering emulsions? Soft Matter 8, 5233–5240. https://doi.org/10.1039/C2SM07230K.
Bai, B., Han, M., Li, Y., Wei, M., Gao, Y., Coste, J.P., 2000. Selective water shutoff technology study and application of W/O emulsions. In: SPE Conference of Improved Oil Recovery Symposium. https://doi.org/10.2118/59320-MS.
Barnes, H.A., 1994. Rheology of emulsions—a review. Colloids Surf. A Physicochem. Eng. Asp. 91, 89–95. https://doi.org/10.1016/0927-7757(93)02719-U.
Bizmark, N., Du, X., Ioannidis, M.A., 2020. High internal phase Pickering emulsions as templates for a cellulosic functional porous material. ACS Sustain. Chem. Eng. 8, 3664–3672. https://doi.org/10.1021/acssuschemeng.9b06577.
Chen, D., Zhao, H., Liu, K., Huang, Y., Li, B., 2021. The effect of emulsion and foam on anti-water coning during nitrogen foam injection in bottom-water reservoirs. J. Petrol. Sci. Eng. 196, 107766. https://doi.org/10.1016/j.petrol.2020.107766.
Chen, L., Zhang, G., Ge, J., Jiang, P., Liu, Y., Ran, Y., 2014. Property evaluation of a new selective water shutoff agent for horizontal well. Colloids Surf. A Physicochem. Eng. Asp. 446, 33–45. https://doi.org/10.1016/j.colsurfa.2014.01.035.
Chen, X., Wu, F., Tang, J., Yang, K., Ma, Y., Pan, J., 2020. Anisotropic emulsion constructed boronate affinity imprinted Janus nanosheets for stir bar sorptive extraction of *cis*-diol-containing catechol. Chem. Eng. J. 395, 124995. https://doi.org/10.1016/j.cej.2020.124995.
Chen, Y., Liang, F., Yang, H., Zhang, C., Wang, Q., Qu, X., Li, J., Cai, Y., Qiu, D., Yang, Z., 2012. Janus nanosheets of polymer–inorganic layered composites. Macromolecules 45, 1460–1467. https://doi.org/10.1021/ma2021908.
Crespo, F., Reddy, B., Eoff, L., Lewis, C., Pascarella, N., 2014. Development of a polymer gel system for improved sweep efficiency and injection profile modification of IOR/EOR treatments. In: International Petroleum Technology Conference. https://doi.org/10.3997/2214-4609-pdb.395.IPTC-17226-MS.
Cui, J., 2015. Study on screening and applying of selective water shutoff agent for horizontal well. In: International Conference on Chemical, Material and Food Engineering, pp. 381–384. https://doi.org/10.2991/cmfe-15.2015.90.
Cui, S., Yang, Z., McClements, D.J., Xu, X., Qiao, X., Zhou, L., Sun, Q., Jiao, B., Wang, Q., Dai, L., 2023. Stability mechanism of Pickering emulsions co-stabilized by protein nanoparticles and small molecular emulsifiers by two-step emulsification with different adding sequences: from microscopic to macroscopic scales. Food Hydrocolloids 137, 108372. https://doi.org/10.1016/j.foodhyd.2022.108372.
Cui, Y., Tan, Z., An, C., 2022. Research and application of multi-functional acrylic resin grouting material. Construct. Build. Mater. 359, 129381. https://doi.org/10.1016/j.conbuildmat.2022.129381.
Eyring, H., 1935. The activated complex and the absolute rate of chemical reactions. Chem. Rev. 17, 65–77. https://doi.org/10.1021/cr60056a006.
Eyring, H., 2004. The activated complex in chemical reactions. J. Chem. Phys. 3, 107–115. https://doi.org/10.1063/1.1749604.
Ghannam, M.T., 2005. Water-in-crude oil emulsion stability investigation. Petrol. Sci. Technol. 23, 649–667. https://doi.org/10.1081/LFT-200033001.
Glaser, N., Adams, D.J., Böker, A., Krausch, G., 2006. Janus particles at liquid-liquid interfaces. Langmuir 22, 5227–5229. https://doi.org/10.1021/la060693i.
Hill, F., Monroe, S., Mohanan, R., 2012. Water management—an increasing trend in

the oil and gas industry. In: SPE/EAGE European Unconventional Resources Conference and Exhibition. https://doi.org/10.2118/154720-MS.
Horozov, T.S., Aveyard, R., Binks, B.P., Clint, J.H., 2005. Structure and stability of silica particle monolayers at horizontal and vertical octane-water interfaces. Langmuir 21, 7405–7412. https://doi.org/10.1021/la050923d.
Hu, J., Zhou, S., Sun, Y., Fang, X., Wu, L., 2012. Fabrication, properties and applications of Janus particles. Chem. Soc. Rev. 41, 4356–4378. https://doi.org/10.1039/C2CS35032G.
Jia, H., Dai, J., Miao, L., Wei, X., Tang, H., Huang, P., Jia, H., He, J., Lv, K., Liu, D., 2021. Potential application of novel amphiphilic Janus-SiO_2 nanoparticles stabilized O/W/O emulsion for enhanced oil recovery. Colloids Surf. A Physicochem. Eng. Asp. 622, 126658. https://doi.org/10.1016/j.colsurfa.2021.126658.
Jin, Z., Wang, Y., Liu, J., Yang, Z., 2008. Synthesis and properties of paraffin capsules as phase change materials. Polymer 49, 2903–2910. https://doi.org/10.1016/j.polymer.2008.04.030.
Kabir, A.H., 2001. Chemical water & gas shutoff technology—an overview. In: SPE Asia Pacific Improved Oil Recovery Conference. https://doi.org/10.2118/72119-MS.
Kadeethum, T., Sarma, H.K., Maini, B.B., 2017. Enhance microscopic sweep efficiency by smart water in tight and very tight oil reservoirs. In: SPE Unconventional Resources Conference. https://doi.org/10.2118/185032-MS.
Kawazoe, A., Kawaguchi, M., 2011. Characterization of silicone oil emulsions stabilized by TiO_2 suspensions pre-adsorbed SDS. Colloids Surf. A Physicochem. Eng. Asp. 392, 283–287. https://doi.org/10.1016/j.colsurfa.2011.10.005.
Kolotova, D.S., Kuchina, Y.A., Petrova, L.A., Voron'ko, N.G., Derkach, S.R., 2018. Rheology of water-in-crude oil emulsions: influence of concentration and temperature. Colloids and Interfaces 2, 64. https://doi.org/10.3390/colloids2040064.
Kumar, A., Mandal, A., 2017. Synthesis and physiochemical characterization of zwitterionic surfactant for application in enhanced oil recovery. J. Mol. Liq. 243, 61–71. https://doi.org/10.1016/j.molliq.2017.08.032.
Kumar, A., Park, B.J., Tu, F., Lee, D., 2013. Amphiphilic Janus particles at fluid interfaces. Soft Matter 9, 6604–6617. https://doi.org/10.1039/C3SM50239B.
Lai, N., Fan, S., Zhao, W., Xu, H., 2022. Development and performance of urea-formaldehyde resin/montmorillonite intercalation composite horizontal well plugging agent. Chem. Technol. Fuels Oils 58, 157–168. https://doi.org/10.1007/s10553-022-01363-x.
Li, G., Fu, M., Li, X., Hu, J., 2022. A Study of the thin film-coated swelling retarding particles in fractured carbonate reservoirs for water plugging and profile control. Energies 15, 1085. https://doi.org/10.3390/en15031085.
Liu, F., Xu, J., Tan, S., Gong, A., Li, H., 2022. Orthogonal experiments and neural networks analysis of concrete performance. Water 14, 2520. https://doi.org/10.3390/w14162520.
Liu, J., Wang, X., Cheng, H., Fan, H., 2023. Orthogonal design and microstructure mechanism analysis of novel bentonite polymer slurry in pipe jacking. Polymers 15, 1461. https://doi.org/10.3390/polym15061461.
Liu, R., Lu, J., Pu, W., Xie, Q., Lu, Y., Du, D., Yang, X., 2021. Synergetic effect between in-situ mobility control and micro-displacement for chemical enhanced oil recovery (CEOR) of a surface-active nanofluid. J. Petrol. Sci. Eng. 205, 108983. https://doi.org/10.1016/j.petrol.2021.108983.
Liu, R., Xu, Y., Pu, W., Yang, X., Varfolomeev, M.A., Zou, B., He, M., Gou, R., 2023. A universal route to deciphering the internal mechanism of crude oil self-emulsification. J. Mol. Liq. 383, 122165. https://doi.org/10.1016/j.molliq.2023b.122165.
Di Lullo, G., Rae, P., Curtis, J., 2002. New insights into water control—a review of the state of the art - Part II. In: SPE International Thermal Operations and Heavy Oil Symposium and International Horizontal Well Technology Conference. https://doi.org/10.2118/77963-MS.
McAuliffe, C.D., 1973a. Crude-oil-water emulsions to improve fluid flow in an oil reservoir. J. Petrol. Technol. 25, 721–726. https://doi.org/10.2118/4370-PA.
McAuliffe, C.D., 1973b. Oil-in-water emulsions and their flow properties in porous media. J. Petrol. Technol. 25, 727–733. https://doi.org/10.2118/4369-PA.
Moradi, M., Kazempour, M., French, J.T., Alvarado, V., 2014. Dynamic flow response of crude oil-in-water emulsion during flow through porous media. Fuel 135, 38–45. https://doi.org/10.1016/j.fuel.2014.06.025.
Nonomura, Y., Komura, S., Tsujii, K., 2004. Adsorption of disk-shaped Janus beads at liquid–liquid interfaces. Langmuir 20, 11821–11823. https://doi.org/10.1021/la0480540.
Pang, X., Wan, C., Wang, M., Lin, Z., 2014. Strictly biphasic soft and hard Janus structures: synthesis, properties, and applications. Angew. Chem. Int. Ed. 53, 5524–5538. https://doi.org/10.1002/anie.201309352.
Perles, C.E., Guersoni, V.C.B., Bannwart, A.C., 2018. Rheological study of crude oil/water interface—the effect of temperature and brine on interfacial film. J. Petrol. Sci. Eng. 162, 835–843. https://doi.org/10.1016/j.petrol.2017.11.010.
Romero, L., Ziritt, J.L., Marin, A., Rojas, F., Mogollon, J.L., Paz, E.M.F., 1996. Plugging of high permeability—fractured zones using emulsions. In: SPE/DOE Improved Oil Recovery Symposium. https://doi.org/10.2118/35461-MS.
Seddiqi, K.N., Abe, K., Hao, H., Mahdi, Z., Liu, H., Hou, J., 2023. Optimization and performance evaluation of a foam plugging profile control well selection system. ACS Omega 8, 10342–10354. https://doi.org/10.1021/acsomega.2c08002.
Seright, R.S., Lane, R.H., Sydansk, R.D., 2003. A strategy for attacking excess water production. SPE Prod. Facil. 18, 158–169. https://doi.org/10.2118/84966-PA.
Shams, S.M., Dehghan, A.A., Kazemzadeh, Y., Riazi, M., 2024. Experimental investigation of emulsion formation and stability: comparison of low salinity water and smart water effect. J. Dispersion Sci. Technol. 45 (8), 1646–1655. https://doi.org/10.1080/01932691.2023.2225612.
Song, X., Zhao, M., Dai, C., Wang, X., Lv, W., 2021. Mechanism of active silica nanofluids based on interface-regulated effect during spontaneous imbibition. Petrol. Sci. 18, 883–894. https://doi.org/10.1007/s12182-020-00537-8.
Song, Y., Chen, S., 2014. Janus nanoparticles: preparation, characterization, and applications. Chem. Asian J. 9, 418–430. https://doi.org/10.1002/asia.201301398.
Soo, H., Radke, C.J., 1984a. Flow mechanism of dilute, stable emulsions in porous media. Ind. Eng. Chem. Fundam. 23, 342–347. https://doi.org/10.1021/i100015a014.
Soo, H., Radke, C.J., 1984b. Velocity effects in emulsion flow through porous media. J. Colloid Interface Sci. 102, 462–476. https://doi.org/10.1016/0021-9797(84)90249-2.
Tang, W., Zou, C., Liang, H., Da, C., Zhao, Z., 2022. The comparison of interface properties on crude oil-water and rheological behavior of four polymeric nanofluids (nano-SiO_2, nano-CaO, GO and CNT) in carbonates for enhanced oil recovery. J. Petrol. Sci. Eng. 214, 110458. https://doi.org/10.1016/j.petrol.2022.110458.
Tong, L., Fan, R., Yang, S., Zhang, Q., Pan, Y., 2022. Experimental study of oilfield water plugging with organic chromium gel. Chem. Technol. Fuels Oils 57, 991–999. https://doi.org/10.1007/s10553-022-01336-0.
Vidrine, W.K., Willson, C.S., Valsaraj, K.T., 2000. Emulsions in porous media. I. Transport and stability of polyaphrons in sand packs. Colloids Surf. A Physicochem. Eng. Asp. 175, 277–289. https://doi.org/10.1016/S0927-7757(00)00429-5.
Wang, Z., Li, Z., Fu, S., He, H., Chen, A., Zhai, D., 2021. Experimental study of the plugging—matching relationship between elastic particles and formation pore throats. J. Dispersion Sci. Technol. 42, 190–205. https://doi.org/10.1080/01932691.2019.1667819.
Wijeratne, D.I.E.N., Halvorsen, B.M., 2015. Computational study of fingering phenomenon in heavy oil reservoir with water drive. Fuel 158, 306–314. https://doi.org/10.1016/j.fuel.2015.05.052.
Xiang, D., Jiang, B., Liang, F., Yan, L., Yang, Z., 2020. Single-chain Janus nanoparticle by metallic complexation. Macromolecules 53, 1063–1069. https://doi.org/10.1021/acs.macromol.9b02388.
Xie, S., Chen, S., Zhu, Q., Li, X., Wang, D., Shen, S., Jin, M., Zhou, G., Zhu, Y., Shui, L., 2020. Janus nanoparticles with tunable amphiphilicity for stabilizing Pickering-emulsion droplets via assembly behavior at oil–water interfaces. ACS Appl. Mater. Interfaces 12, 26374–26383. https://doi.org/10.1021/acsami.0c05625.
Xu, X., Liu, Y., Gao, Y., Li, H., 2017. Preparation of Au@silica Janus nanosheets and their catalytic application. Colloids Surf. A Physicochem. Eng. Asp. 529, 613–620. https://doi.org/10.1016/j.colsurfa.2017.06.048.
Yang, J.P., 2014. Visualization experimental study on organic-inorganic crosslinked plugging system plugging. Adv. Mater. Res. 868, 574–579. https://doi.org/10.4028/www.scientific.net/AMR.868.574.
Yu, L., Ding, B.X., Dong, M.Z., Jiang, Q., 2018a. Plugging ability of oil-in-water emulsions inporous media: experimental and modeling study. Ind. Eng. Chem. Res. 57 (43), 14795–14808. https://doi.org/10.1021/acs.iecr.8b03805.
Yu, L., Dong, M., Ding, B., Yuan, Y., 2018b. Emulsification of heavy crude oil in brine and its plugging performance in porous media. Chem. Eng. Sci. 178, 335–347. https://doi.org/10.1016/j.ces.2017.12.043.
Yu, L., Li, S., Stubbs, L.P., Lau, H.C., 2021. Characterization of clay-stabilized, oil-in-water Pickering emulsion for potential conformance control in high-salinity, high-temperature reservoirs. Appl. Clay Sci. 213, 106246. https://doi.org/10.1016/j.clay.2021.106246.
Yuan, Z., Cao, Z., Wu, R., Xu, Q., Xu, H., Wu, H., Jin, B., Wu, W., Zheng, J., Wu, J., 2023. Mechanically robust and rapidly degradable hydrogels for temporary water plugging in oilfields. J. Polym. Sci. 61, 262–270. https://doi.org/10.1002/pol.20220495.
Yue, L., Pu, W., Zhao, T., Zhuang, J., Zhao, S., 2022. A high performance magnetically responsive Janus nano-emulsifier: preparation, emulsification characteristics, interfacial rheology, and application in emulsion flooding. J. Petrol. Sci. Eng. 208, 109478. https://doi.org/10.1016/j.petrol.2021.109478.
Zahn, N., Kickelbick, G., 2014. Synthesis and aggregation behavior of hybrid amphiphilic titania Janus nanoparticles via surface-functionalization in Pickering emulsions. Colloids Surf. A Physicochem. Eng. Asp. 461, 142–150. https://doi.org/10.1016/j.colsurfa.2014.07.039.
Zhang, Y., Cai, H., Li, J., Cheng, R., Wang, M., Bai, X., Liu, Y., Sun, Y., Dai, C., 2018. Experimental study of acrylamide monomer polymer gel for water plugging in low temperature and high salinity reservoir. Energy Sources, Part A Recovery, Util. Environ. Eff. 40, 2948–2959. https://doi.org/10.1080/15567036.2018.1514436.
Zhang, Z., Cao, G., Zuo, J., Bai, Y., 2020. Rheological properties and plugging behavior of active crude oil. Petrol. Sci. Technol. 38, 131–145. https://doi.org/10.1080/10916466.2019.1690508.
Zhou, Y., Wang, D., Wang, Z., Cao, R., 2017. The formation and viscoelasticity of pore-throat scale emulsion in porous media. Petrol. Explor. Dev. 44, 111–118. https://doi.org/10.1016/S1876-3804(17)30014-9.